remote sensing

MDPI

Article

Seasonal Variation of Stratospheric Gravity Waves in the Asian Monsoon Region Derived from COSMIC-2 Data

Tao Qu, Lifeng Zhang *, Yuan Wang, Xu Wang and Jiping Guan

Department of Atmosphere Science and Engineering, College of Meteorology and Oceanography, National University of Defense Technology, Changsha 410073, China
* Correspondence: zhanglifeng@nudt.edu.cn; Tel.: +86-135-1254-9105

Abstract: COSMIC-2 (Constellation Observing System for Meteorology, Ionosphere and Climate-2) dry temperature profile data from December 2019 to November 2021 are used to study stratospheric gravity waves (GWs) in the Asian monsoon region. The stratosphere between 20 and 50 km is divided into the lower, middle, and high layers based on the vertical distribution of the mean potential energy (Ep) and the horizontal distribution of GW Ep in these three layers, and their seasonal changes are analyzed. The source and propagating mechanism of GWs in middle latitudes in winter are revealed. The results show that GWs in the stratosphere have distinct distribution features during different seasons. The significant Ep in winter appears mainly in middle latitudes north of 30°N, whereas in summer, it appears in the low latitudes south of 30°N. There are significant areas of GW activity in both low and middle latitudes in spring and autumn, but their intensity is significantly weaker than in winter and summer. Areas with significant GWs and the seasonal variation of their intensity are accompanied by the Asian monsoon activity. In winter, there is a northward and upward propagating column for GWs above the Sichuan Basin, and in summer, there is an eastward and upward propagating column for GWs in the zonal band 15–25°N. The occurrence of GWs in northwestern China in winter is the result of the subtropical jet stream and topography. Once GWs enter the stratosphere, they are regulated by the winter stratospheric environment, and the GWs acquire a northerly component by the wind shear. The meridional wind shear in the background field is an important factor affecting the development and propagation of GWs.

Keywords: stratospheric gravity waves; COSMIC-2 data; potential energy; Asian monsoon region

check for updates

Citation: Qu, T.; Zhang, L.; Wang, Y.; Wang, X.; Guan, J. Seasonal Variation of Stratospheric Gravity Waves in the Asian Monsoon Region Derived from COSMIC-2 Data. *Remote Sens.* **2022**, *14*, 4096. https://doi.org/10.3390/rs14164096

Academic Editor: Michael E. Gorbunov

Received: 21 July 2022
Accepted: 19 August 2022
Published: 21 August 2022

1. Introduction

Gravity waves (GWs) transport energy, momentum, and chemical and atmospheric constituents horizontally and vertically, and they play a major role in atmospheric dynamics and global atmospheric circulation [1]. General circulation models cannot resolve the effects of small-scale GWs; thus, a GW parameterization scheme must be introduced into models to obtain a reasonable circulation pattern and thermal structure. The absence of long-term and stable global GW observations means that GW parameterization schemes still lack physical verification [2]. Therefore, continuous and stable observations of GWs over larger geographical areas are essential for deepening the understanding of the characteristics of GWs, as well as for improving GW parameterization schemes in numerical models [3].

At present, a variety of observational data have been used in the study of atmospheric GWs. Among them, the more mature technologies are ground-based observations, such as radiosonde [4], radar [5], superpressure balloon [6,7], and sounding rockets [8]. However, ground-based observations are severely limited by the geographical distribution of observation stations, and it is difficult to obtain high-resolution observational data for larger geographical areas. With the development of satellite atmospheric sounding technology, it has become possible to obtain the global distribution of GWs, and Global Positioning

System (GPS) radio occultation (RO) has received increasing attention. In a neutral atmosphere, the atmospheric reflectivity obtained by GPS RO can provide further data such as temperature, pressure, and water vapor content [9]. At present, GPS RO atmospheric sounding systems include GPS/Meteorology [10], Challenge Minisatellite Payload [11], and COSMIC (Constellation Observing System for Meteorology, Ionosphere and Climate) [12]. Of these systems, the COSMIC satellite data have higher temporal and spatial density. The COSMIC satellite system consists of six low-orbit satellites launched in California in April 2006, with an orbital inclination of 72° and an operating height of 800 km, providing more than 2000 detection profiles every day around the world. For more information about COSMIC satellites, please refer to Anthes et al. [9].

GPS RO data have been widely used in the study of atmospheric GWs in recent years. Tsuda et al. [13] calculated the global distribution of stratospheric GW potential energy (Ep) using GPS/Meteorology (GPS/MET) data. However, the GPS/MET satellite provides only 100–150 temperature profiles per day worldwide, and detailed distribution features of GW Ep cannot be acquired. Xu et al. [14] obtained the global distribution and seasonal variation of GW Ep in the 20–30 km height layer using COSMIC RO data with 2000 temperature profiles every day from 2006 to 2013. They found that high values of Ep occur at the equator and decrease toward the poles, which is similar to the result of Tsuda et al. [13] using GPS/MET satellite data. Xu et al. [14] also found that the Ep of the whole winter hemisphere is higher than that of the summer hemisphere, and the GW intensity in the Southern Hemisphere winter is greater than that in the Northern Hemisphere winter. Because the COSMIC satellites were in a cluster formation from 2006 to 2007, Wang and Alexander [15] further obtained the global distribution of wave parameters such as the amplitude, vertical wavelength, horizontal wavelength, momentum flux, and intrinsic frequency of stratospheric GWs using the least-squares method by taking advantage of the high resolution at this stage of the mission. Using COSMIC data as well, Faber et al. [16] obtained more accurate wave parameter distribution characteristics by improving the phase difference method and reported that GWs have larger wave amplitudes and longer horizontal wavelengths in the equatorial region as well as longer vertical wavelengths at middle and high latitudes compared with the equatorial region. They also found that the distribution of momentum flux is similar to that of Ep.

The COSMIC satellite data can be used not only for the observation of GWs on a global scale but also to study GWs in specific regions. Hindley et al. [17] found that orographic GWs generated in the Southern Andes spread to the center of the jet stream of the middle and upper stratosphere. Šácha et al. [18] found strong GW activity over the Sea of Japan in October and November. However, the resolution in previous studies could only reach $5° \times 5°$ based on the current density of COSMIC RO data, and it was difficult to obtain a more detailed regional GW distribution. Therefore, most previous studies were on the global scale, and there are relatively few studies of the Asian monsoon region.

Following the launch of the COSMIC satellite system, the COSMIC-2 (Constellation Observing System for Meteorology, Ionosphere and Climate-2) satellite system was launched at the Kennedy Space Center in July 2019. It also consists of six low-orbit satellites, with an orbital inclination of 24° and an operating height of 550 km. Each satellite tracks occulting GPS satellites as they rise above or set below the Earth's horizon. As the GPS signal traverses the atmospheric limb, phase delay measurements attributable to changing vertical gradients of refractivity in the atmosphere are measured [17]. Taking an integral along the line of sight, vertical profiles of dry temperature and pressure can be computed at the tangent point of the occultation via an Abel inversion [19]. The dry temperature is the temperature profile that water vapor is not considered in the retrieval of original satellite data and its conversion breaks down in the presence of water vapor but works well in the stratosphere, where water vapor is negligible. Ho et al. [20] estimated a temperature retrieval accuracy of 0.2 K between 8 and 35 km for COSMIC-2. Scheiner et al. [21] found that the bending angle and reflectivity of COSMIC-2 have small errors compared with radiosondes, short-term operational forecasts, and the MERRA-2 from about 2–40 km. In the 45°S–45°N region, COSMIC-2 can provide more than 5000 profiles per day. COSMIC-2 provides a higher horizontal resolution of observations in tropical and mid-latitude areas than COSMIC; thus, COSMIC-2 data are better for GW observation and the study of the characteristics of GW variability. More information about the COSMIC-2 satellite may be found in the work of Schreiner et al. [21].

The combined effects of the Tibetan Plateau, the Pacific Ocean, the Indian Ocean, and the Eurasian continent make the Asian monsoon region one of the most significant monsoon regions in the world, where the circulation and precipitation change significantly with the season. The movement of the subtropical high and the transport of water vapor during the summer monsoon result in significant rainy seasons over the Indian Peninsula, the Indo-China Peninsula, the South China Sea, and the eastern part of China during the summer monsoon. The complex topography of the Asian monsoon region, the significant seasonally movement of the subtropical jet stream, and the precipitation are all important triggering factors for stratospheric GWs; thus, the Asian monsoon region is a region worthy of attention in the study of regional GW characteristics. Some studies have focused on the spatial distribution and seasonal changes of stratospheric GWs in China [22–24], and others have focused on the basic characteristics of GWs during particular weather systems [25,26]. However, most of them are based on radiosonde data and numerical simulation results. The simulation results of the numerical model are not exactly consistent with the real atmosphere; that is, the simulation results are different from the observations. These differences are considered a model error. This error is inevitable. The low horizontal resolution of radiosonde data and the inevitable errors of numerical models mean that the universality of the regional stratospheric GWs features revealed by these two methods remains unclear. COSMIC-2 can provide large-area and high-resolution observations of the Asian monsoon region, and these observations with high temporal and spatial coverage have laid the foundation for the study of GWs in this region. Thus far, there have been a few studies [27] on the distribution of stratospheric GWs in the Asian monsoon region based on COSMIC-2 data.

Using the COSMIC-2 vertical temperature profile data for the past two years, this paper studies the activity of stratospheric GWs in the Asian monsoon region and analyzes the characteristics and causes of the spatial and temporal distribution of GWs in the region. This paper is organized as follows: Section 2 introduces the data and method for extracting GWs, Section 3.1 reveals the horizontal and vertical distribution of stratospheric GWs, Section 3.2 analyzes the source and the propagation mechanism of GWs, and Section 4 gives a summary.

2. Data and Method

2.1. Data

The data used in this study are the COSMIC-2 level 2 dry temperature profiles produced by the COSMIC Data Analysis and Archive Center (CDAAC), and the period is 24 months from December 2019 to November 2021. The data download website is https://cdaac-www.cosmic.ucar.edu/ (accessed on 1 March 2022). The study area is the Asian monsoon region, and the specific domain studied in this paper is 70–150°E, 15–45°N. Figure 1 presents the monthly mean sampling density distribution of vertical dry temperature profiles of COSMIC-2 in the study area with a grid resolution of 2.5° × 2.5°. In the latitude range 15–30°N, the monthly mean sampling density is more than 25 in general; in the area north of 30°N, it is about 15. Hindley et al. [17] mentioned that near 30°E and with a grid resolution of 5° × 5°, there are about 20 COSMIC vertical profiles per month, and its sampling density is much smaller than that of COSMIC-2 in this paper. Therefore, the COSMIC-2 data with this resolution can be used to study the seasonal variation of stratospheric GWs in the Asian monsoon region. Following Hindley et al. [17], the upper limit of the data height of COSMIC-2 is limited to 50 km. Although temperature profiles from COSMIC typically exhibit increased noise above around 40 km, the increased number of measurements in the month-long time window potentially allows us to resolve large persistent features at higher altitudes [17]. In addition, the wind data used in this study is ERA5 [28] from the monthly averaged data of the European Centre for Medium-Range Weather Forecasts (ECMWF) at a resolution of 0.25° × 0.25° and can be downloaded from https://cds.climate.copernicus.eu/ (accessed on 1 March 2022).

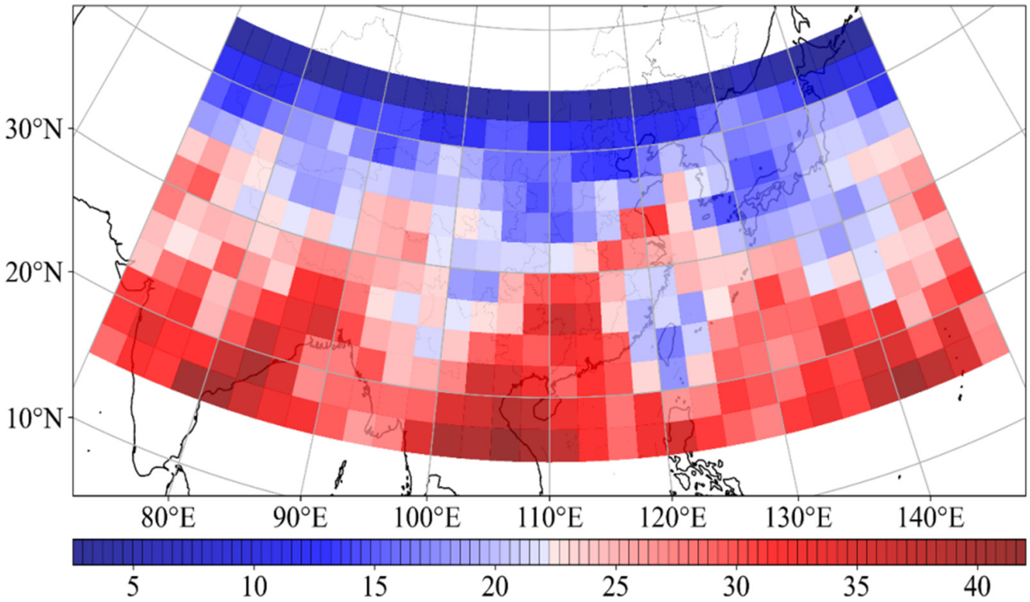

Figure 1. Monthly mean sampling density (unit: number of samples) of COSMIC-2 dry temperature profile data from December 2019 to November 2021 with a grid resolution of 2.5° × 2.5°.

2.2. Method

The properties of GWs can be represented in terms of potential energy (Ep) density per unit mass [13,29]:

$$\mathrm{Ep} = \frac{1}{2}[(\frac{g}{N})^2\overline{(\frac{T'}{T_B})^2}] \tag{1}$$

$$N^2(z) = \frac{g}{T_B}(\frac{\partial T_B}{\partial z} + \frac{g}{C_P}) \tag{2}$$

where T_B is the background temperature, T' is the temperature perturbation, g is the gravitational acceleration, N is the Brunt–Väisälä frequency, C_P is the heat capacity at constant pressure, and Ep is the potential energy of a profile.

For the purpose of calculating Ep, the original observational data need to be processed as follows:

(1) The observed temperature data are linearly interpolated onto equidistant points with a vertical interval of 100 m over heights 9–55 km.

(2) Following Wang and Alexander [15,30], the daily COSMIC-2 temperature profiles are gridded to 10° × 15° latitude–longitude resolution; the mean temperature $\overline{T}$ is the average of all temperature profiles within a grid box.

(3) The background temperature for the gridded data is calculated using $\overline{T}$ based on the following formula, where the coefficients are obtained by the least-squares method according to John and Kumar [31]:

$$T_B = A_0 + \sum_{i=1}^{6} A_i \sin(i\lambda) + \sum_{i=1}^{6} B_i \cos(i\lambda) \tag{3}$$

where T_B is the background temperature at a specific height and latitude, λ is the longitude of the grid point. It can be seen from Equation (3) that the background temperature includes the temperature of planetary waves with zonal wavenumbers of 0 to 6, and $\sqrt{A_i{}^2 + B_i{}^2}$ is the temperature amplitude of the planetary wave. The temperature perturbation is the difference between the observed temperature and the background temperature, $\hat{T} = T - T_B$.

(4) The temperature perturbation is filtered and smoothed in the vertical direction to obtain the GW temperature [13]. The temperature perturbation is first filtered with a bandwidth of 2–10 km according to Tsuda et al. [13] in the vertical direction, and each filtered temperature profile $\hat{T}_{2-10}$ is then smoothed with a vertical height window of 2 km, as follows:

$$\overline{(T')^2} = \frac{1}{z_1 - z_2} \int_{z_1}^{z_2} \hat{T}_{2-10}(z)^2 dz \tag{4}$$

where z_1 and z_2 are the upper and lower heights of the smoothing window, respectively.

(5) Finally, the results of Equations (2) and (4) are inserted into Equation (1) to obtain the vertical profile of Ep. The Ep of the horizontal distribution is obtained by the IDW (inverse distance weight) [32].

3. Results and Discussion

3.1. Spatial Distribution and Seasonal Variation of Stratospheric GWs

Figure 2 shows the variation of regionally and seasonally averaged GW Ep. It is shown that the vertical distribution of Ep varies with height. In Figure 2, the variability of Ep with height is basically the same in the four seasons, and the error bar (Figure 2b) represents the standard deviation, reflecting the degree of dispersion of the data set relative to the mean. From the variability of standard deviation, the dispersion degree of Ep distribution in each season decreases with height, and the dispersion degree of Ep distribution in summer is the largest, especially in the lower stratosphere. At heights of 20–22 km, Ep decreases linearly with height, but it shows oscillatory behavior within the range of 22–30 km. Between 30 and 42 km, Ep again decreases linearly with height and reaches a minimum value around 42 km; from 42 to 50 km, Ep generally increases with height, reaching a maximum value at 50 km. Note that there are obvious maximum and minimum points near 30 and 42 km, respectively. Therefore, given the vertical variation in the distribution of Ep above, the stratosphere between 20 and 50 km is divided into lower (20–30 km), middle (30–42 km), and upper (42–50 km) layers in this study.

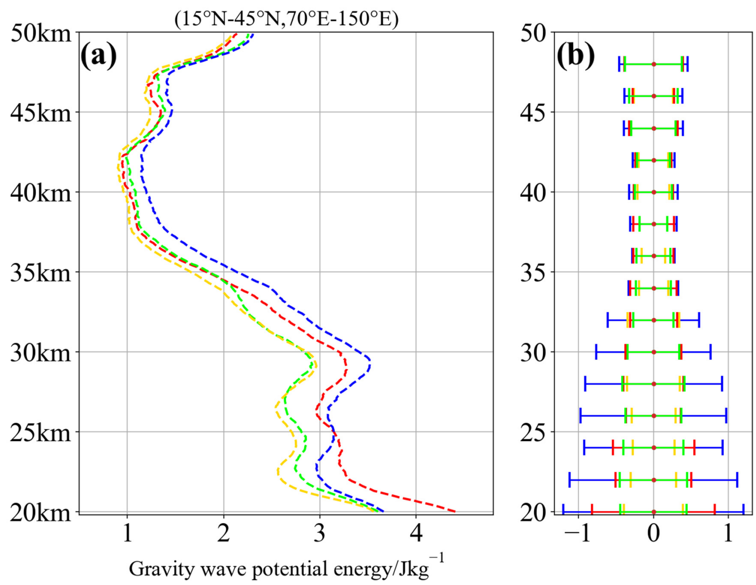

Figure 2. (**a**) Regional seasonal mean profiles of Ep for winter (DJF; December–January–February), spring (MAM; March–April–May), summer (JJA; June–July–August), and autumn (SON; September–October–November). (**b**) The standard deviation relative to the mean at each height (the absolute value of the length of the error bar is twice the standard deviation).

3.1.1. Horizontal Distribution and Seasonal Variation of Ep

Figures 3–5 present the seasonal mean distribution of Ep in the lower, middle, and upper stratosphere, respectively, as defined above. Here, we give a detailed analysis of the distribution and seasonal variation of the characteristics of GWs in the three layers of the stratosphere. To better quantify the analysis, the mean and standard deviation of the Ep were calculated. Referring to Wang et al. [33], we define Ep as greater than the sum of the mean and the standard deviations as "significant Ep"; meanwhile, we define 15–30°N as the low-latitude region and 30–45°N as the mid-latitude region in the following discussion.

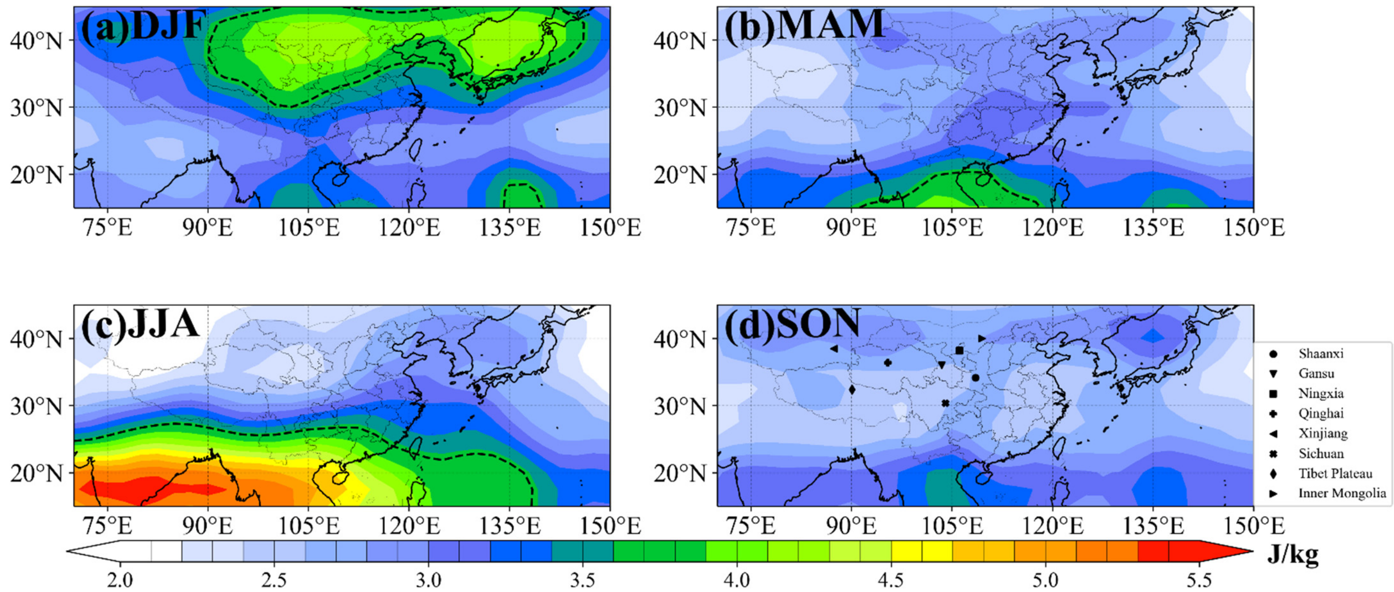

Figure 3. Seasonal mean distribution of Ep in the lower stratosphere. (**a**) DJF, (**b**) MAM, (**c**) JJA, and (**d**) SON, where the dotted line is the sum of the mean and standard deviation of the four seasons Ep.

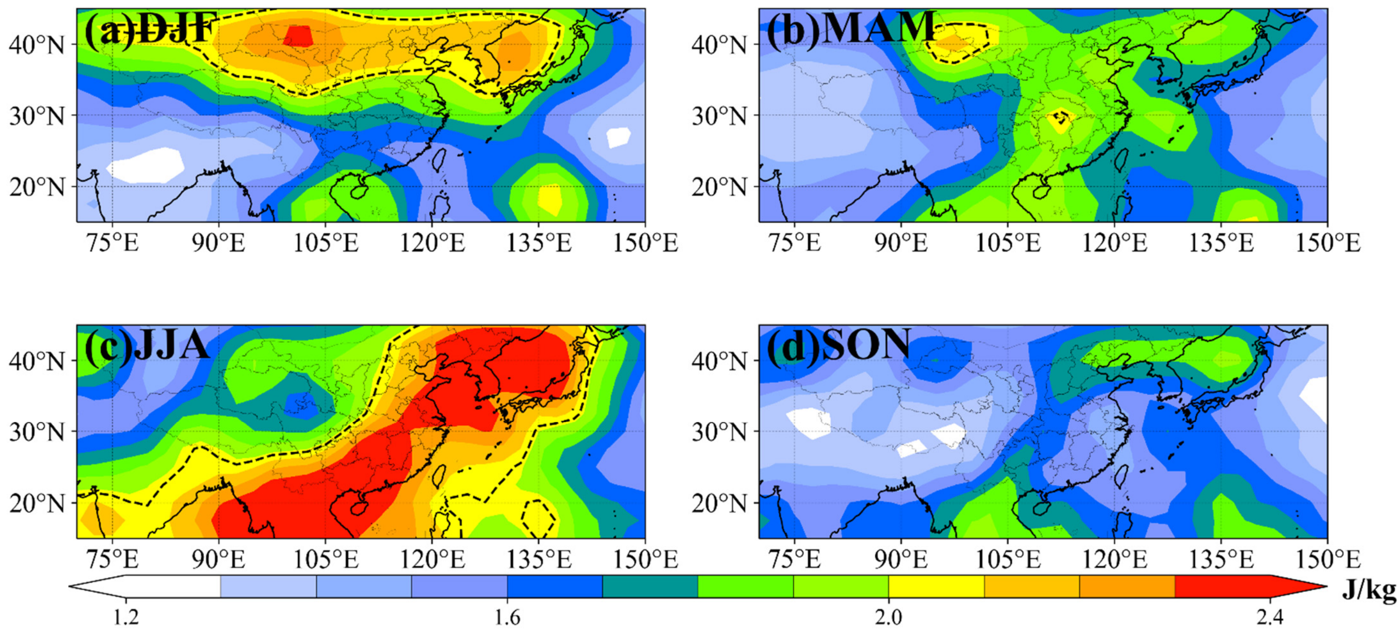

Figure 4. Same as Figure 3, but for the middle stratosphere. (**a**) DJF, (**b**) MAM, (**c**) JJA, and (**d**) SON.

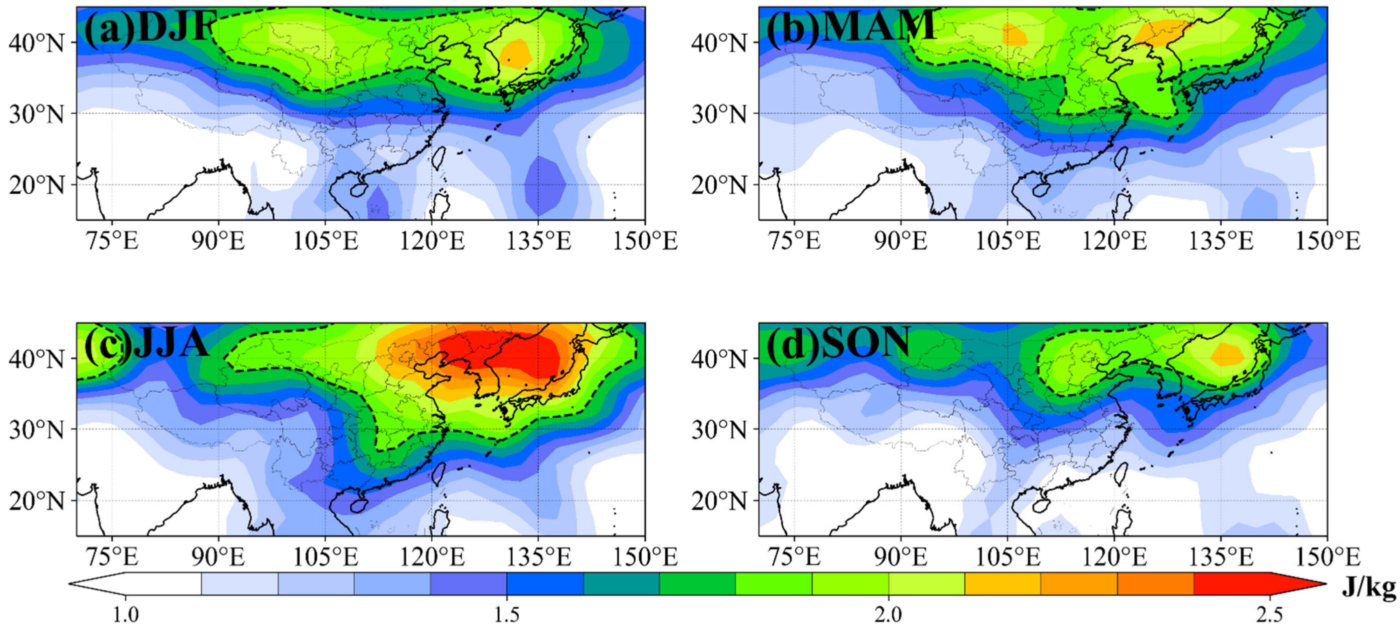

Figure 5. Same as Figure 3, but for the upper stratosphere. (**a**) DJF, (**b**) MAM, (**c**) JJA, and (**d**) SON.

Figure 3 shows the distribution of Ep in the lower stratosphere in four seasons. The regional average Ep values in winter, spring, summer and autumn are 3.29, 2.86, 3.22 and 2.78 Jkg^{-1}, respectively. The standard deviation of Ep for the four seasons is 0.44, 0.39[1], 3.22 and 0.28 Jkg^{-1}, respectively. The part surrounded by dotted lines in Figure 3 represents "significant Ep" in the lower stratosphere with a value of 3.66 Jkg^{-1}. The magnitude of Ep is relatively stronger in winter and summer, and 30°N is a key latitude, with Ep having different distribution features in different seasons on either side of 30°N. In winter, significant Ep appears in the mid-latitude region north of 30°N and reaches a maximum value of 4.5 Jkg^{-1} near 40°N (Figure 3a), while the Ep in the low latitudes south of 30°N is relatively weak. This indicates that stratospheric GWs are more active in mid-latitude regions in winter, and significant Ep appears over Ningxia, southern Gansu, Shaanxi, and Inner Mongolia in northern China. Moreover, there is a large value center of Ep over the Sea of Japan, which corresponds to strong GW activity. In addition, there are centers of large Ep values greater than 3.2 Jkg^{-1} in the Indo-China Peninsula and the Western Pacific, but their influence region is small, and the value of the Indo-China Peninsula is smaller than the significant Ep limit. Using radiosonde data, Chen et al. [24] also found that GWs in northern China are most active in winter. However, as there are only vertical profile data from 20 observation stations, the detailed spatial distribution of Ep was not obtained in their study.

In summer, significant Ep appears south of 30°N, and the center of high value greater than 5.5 Jkg^{-1} is located over the Indian Peninsula and the Bay of Bengal, and there is significant Ep over southeast China, the South China Sea, and the Indo-China Peninsula. Ep is relatively small in the mid-latitudes. This indicates that GWs are more active in the low latitudes in summer. In a study of the global GW distribution, Faber et al. [16] also found regions with high Ep values over the Indian Peninsula and the Indo-China Peninsula in summer. However, their study focused mainly on the global distribution and did not reveal the Ep features of the Asian monsoon regions in detail. Outside the significant Ep area in eastern China, Ep gradually decreases toward northern China and is distributed in stripes (Figure 3c). The distribution of Ep in the low latitudes and eastern China may be related to convection, which is the main source of GWs over the tropics and low latitudes [11].

In spring and autumn (Figure 3b,d), Ep is smaller than in winter and summer. The significant Ep area in spring (Figure 3b) is located over the Indo-China Peninsula south of 30°N. Due to the small Ep in spring, the significant Ep area only appears in the Indo-

China Peninsula. Outside the significant Ep area, the Ep extends from south to north in southeastern China. There is a sub-maximum zone with the Ep value greater than 3.0 Jkg^{-1} in the middle latitudes around 40°N, which indicates GW activity existence over northwest and northeast China. In autumn (Figure 3d), the Ep distribution is similar to that in spring, with belts of relatively high Ep (larger range in the fall, but less than 3.50 Jkg^{-1}) in the middle and low latitudes. Although there is no significant Ep area in autumn, there are also centers of relatively high Ep over the Indo-China Peninsula and the western Pacific, but they are weaker than in spring, while the Ep intensity in the middle latitudes is generally stronger than in spring.

The seasonal variation of GWs is accompanied by the evolution of Asian monsoon circulation. In mid-May, the East Asian summer monsoon first breaks out over the South China Sea and the Indo-China Peninsula, and the southwesterly flows first appear in these regions. Meanwhile, the western Pacific Ocean is controlled by the subtropical high, with easterly flows on its south side. Such a circulation pattern enhances convective activity and precipitation in these areas, and the accompanying stratospheric GW activity over the Indo-China Peninsula and the South China Sea is strengthened (Figure 3b). The South Asian summer monsoon begins in June, and the rainy season begins in the Indian Peninsula. Accordingly, a belt of high Ep appears over the Indian Peninsula, the Bay of Bengal, the Indo-China Peninsula, and the South China Sea, and the center of maximum Ep in the tropics moves westward from the Indo-China Peninsula to the Indian peninsula (Figure 3c). As the subtropical high moves northward in summer, the rain belt develops in eastern China and extends from south to north, corresponding to the high Ep belt extending from the Indo-China Peninsula to the Korean Peninsula in summer. With the start of autumn, the winter monsoon (summer monsoon) strengthens (weakens), and the subtropical jet stream moves southward relative to summer. Meanwhile, the activity of GWs in low-latitude regions weakens, while the maximum values of Ep along the 40°N belt-like distribution increase significantly, with the maximum value centers over eastern and western Xinjiang and the Sea of Japan. In winter, the subtropical jet stream is at its strongest, as are the mid-latitude GWs around the Sea of Japan and Inner Mongolia. The significant seasonal variation of the Ep distribution indicates that the GW activity in the tropics may be related to strong convection caused by the Asian monsoon, while the GW activity in the mid-latitudes may be related to the movement and changes in the intensity of the subtropical jet stream.

In the middle stratosphere (Figure 4), Ep is in general weaker than in the lower stratosphere, and the average Ep values in winter, spring, summer and autumn are 1.75, 1.68, 2.00 and 1.58 Jkg^{-1} in the middle stratosphere, respectively. The standard deviation of Ep for the four seasons is 0.27, 0.19, 0.29 and 0.16 Jkg^{-1}, respectively. Their distribution has both similarities and differences with respect to that in the lower stratosphere in the four seasons. The part surrounded by dotted lines in Figure 4 represents "significant Ep" with a value of 2.03 Jkg^{-1}. In winter, the significant Ep area over Ningxia clearly moves westward compared with that in the lower stratosphere, which may be related to the strong westerly wind in winter. Owing to the filtering effect of the background wind, GWs tend to propagate westward under the background westerly wind. The center of high Ep value over Japan moves southwest compared with that in the lower stratosphere. In spring, there is a belt of high Ep with a value greater than 1.8 Jkg^{-1} extending from southeastern China to the Korean Peninsula, and another significant Ep region is located over northwestern China, and the intensities of the mid-latitude and low-latitude GWs are roughly equal, unlike the distribution of Ep in the lower stratosphere. Similar to spring, the intensity of GWs in middle latitudes in summer is generally equal to that in low latitudes, and the belt of significant Ep values from the Indo-China Peninsula to the Korean Peninsula is more obvious. The distribution of Ep in autumn shows both winter and summer features, although there is basically no "significant Ep" area that we define in this layer. There are Ep value centers both north and south of 30°N with a value more than 1.8 Jkg^{-1}, and the two high-value centers south of 30°N are the same as in winter, located over the Indo-China Peninsula and the western Pacific. The Ep center in mid-latitudes is located over western

China and the Sea of Japan, and there is an Ep belt from the Indo-China Peninsula to the Sea of Japan in autumn, although it is weaker than in summer.

In the upper stratosphere (Figure 5), the distribution of Ep is quite different from the corresponding results in the lower and middle stratosphere, with the main feature of the distribution of Ep in this layer being the smaller seasonal variation. The average Ep values in winter, spring, summer and autumn are 1.41, 1.46, 1.55 and 1.34 Jkg^{-1}, respectively. The standard deviation of Ep for the four seasons is 0.35, 0.33, 0.41 and 0.32 Jkg^{-1}, respectively. The part surrounded by dotted lines in Figure 5 represents "significant Ep" with a value of 1.80 Jkg-1. The belt of significant Ep is present in all seasons in the middle-latitude region, and the values of Ep are obviously larger than in the low-latitude region. The Ep center is located over the Sea of Japan in all four seasons, and its intensity is greatest in summer. In the lower stratosphere, the activity of GWs over the Sea of Japan is the weakest in summer, which has completely different characteristics from the lower stratosphere. This is an interesting phenomenon, and we will study it in the future. The large value area of Ep in northwestern China does not continue to move westward in the upper stratosphere in winter, which may be due to the effect of the Doppler shift caused by the increase in zonal wind speed with height. In the lower layer in spring (Figure 3b), summer (Figure 3c), and autumn (Figure 3d), the intensity of GWs in the low-latitude regions is significantly greater than in the mid-latitude regions, while this distribution is reversed in the upper layer, indicating that low-latitude GWs are more difficult to propagate to the upper stratosphere than mid-latitude GWs in the 2–10 km filtering range.

3.1.2. Vertical Distribution and Seasonal Variation of Ep

To reveal the latitude–height distribution of GWs in the Asian monsoon region in four seasons, the latitude–height cross section at 100°–115°E is selected for analysis, as there are frequent large Ep values (Figures 3–5), and it is located on the Sichuan Basin. In this meridional belt, the Ep value at each height between 15 and 50 km is averaged in the zonal direction; thus, the variation of Ep with latitude and height is obtained. To clearly show the vertical structure of Ep, following the method of Hindley et al. [17], the Ep values of different latitudes are normalized at each height, so that at the same height, the minimum and maximum Ep values are 0 and 1, respectively.

Figure 6 gives the latitude–height distribution of normalized Ep over this meridional belt for four seasons. In winter (Figure 6a), there is a column of large Ep from 20 to 50 km, but the column is not vertically aligned; namely, the latitude of the large Ep value varies with height. From 20 to 25 km in the lower stratosphere, the maximum value of Ep shifts from 30° to 40°N, which reflects that GWs have both upward-propagating and northward-propagating components in this layer. The lower section of the column moves nearly 900 km northward over the height region between 20 and 25 km. Above 25 km, the column is vertically aligned at fixed latitude, which indicates that the mid-latitude GWs in the 40°N area propagate vertically upward. In a study of the orographic GWs over the Andes Mountains in the Southern Hemisphere in winter using COSMIC data, Hindley et al. [17] found a GW column that slopes upward from 30° to 60° S along the latitude–height cross-section at 65° W (Figure 3 in Hindley et al. [17]). From 22 to 35 km, these Andes GWs propagate southward for 1500 km as they propagate upward, and the GWs begin to propagate vertically upward near the wind velocity core of the westerly jet stream at a height of 35 km. Our result is similar to their study, but the propagation direction is different. The phenomenon of different propagation directions of GWs at different heights may be related to the different spectral parameters of the GWs and the background circulation of the stratosphere. The propagation column in Figure 6a shows that the GW source at 40°N originates from 30°N or even farther south, and the northward propagation in the lower layer may be related to the high wind speed region [17]. Moreover, another mechanism for the formation of a such column of Ep must also be considered. At 22–33°N, the zonal wind decreases with the height above the subtropical jet; thus, there is zero wind speed at 35 km. The GW generated by the subtropical jet stream will be filtered out between 20 and 35 km due to encountering a critical level and inducing GWs drag. In this region (30–35°N, 100–115°E, 20–22 km), the upward group velocity becomes slow, and the gravity wave energy is accumulated. The upward propagation GWs generated by subtropical jets will be filtered by the critical level in this region. Therefore, the Ep maximum value moves from 30–35°N to 35–45°N. This may be the reason for the reduction of the GW intensity above 20 km at 30–35°N and the shift of maximum Ep.

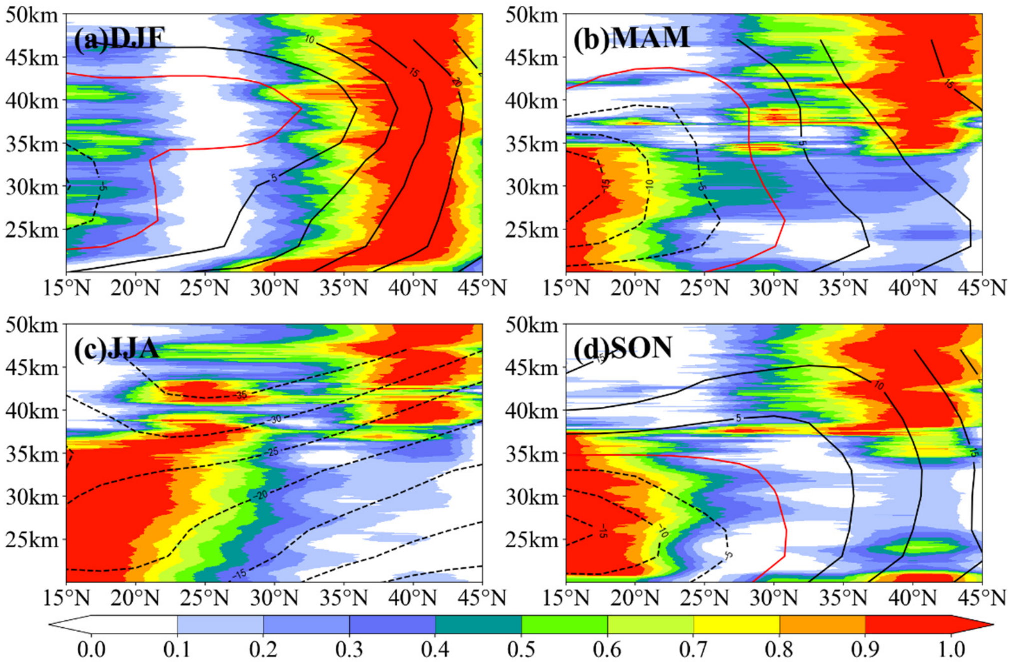

Figure 6. Latitude–height distribution of normalized Ep (shaded) and zonal westerly (solid lines, unit: m s^{-1}) and easterly (dashed lines, unit: m s^{-1}) winds along the seasonal mean of 107.5°E (±7.5°). (**a**) DJF, (**b**) MAM, (**c**) JJA, and (**d**) SON.

In spring, summer, and autumn (Figure 6b–d), the vertical distribution of Ep is different from that in winter, but the vertical structures of Ep in these three seasons are similar; namely, there are two relatively separated areas of high upward-propagating Ep. One is in the low latitudes south of 30°N, within which the maximum value of Ep appears below about 35 km; the other is in the middle latitudes near 40°N, where the maximum value of Ep appears above about 35 km. The two regions with large Ep are discontinuous in height and latitude, and the significant regions of GWs in the middle and low latitudes appear at different heights in these three seasons, which may be related to the different degrees of dissipation of GWs with height in different regions. As mentioned in Section 3.1, low-latitude GWs are stronger in the middle and lower stratosphere, and weaker in the upper stratosphere, whereas mid-latitude GWs tend to propagate to the middle and upper stratosphere.

To reveal the vertical distribution of Ep in the zonal direction, two latitude belts with large Ep values at the middle (30–45°N) and low (15–25°N) latitudes are selected and averaged in the meridional direction and then normalized zonally at each height. As high Ep appears in different regions in different seasons and the Ep in winter and summer is significantly larger than in spring and autumn, Figure 7 only shows the distribution of Ep for mid-latitude winter and low-latitude summer.

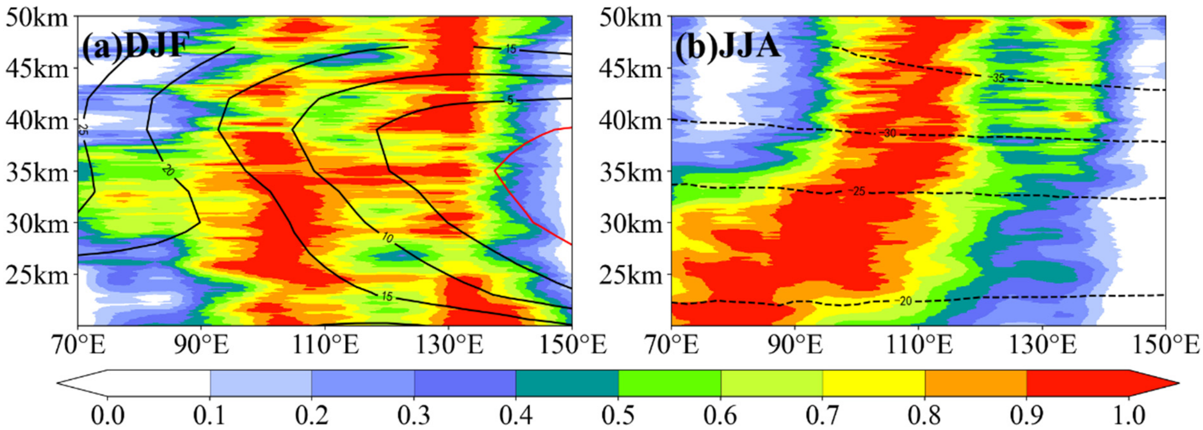

Figure 7. Longitude–height distribution of normalized Ep (shaded) and zonal westerly (solid lines, unit: m s^{-1}) and easterly (dashed lines, unit: m s^{-1}) winds along 40°N (±2.5°) (**a**) and 20°N (±5°) (**b**).

In the winter mid-latitude region (Figure 7a), large Ep mainly appears in two longitude areas, 90–115°E and 130–145°E, which correspond to the significant areas of GWs over northwestern China and the Sea of Japan, respectively. The GWs propagate vertically upward through the entire height range in two columns. The GWs of the eastern column are stronger at heights of 20–25 and 40–50 km than those of the western column, and the GWs of the western column are stronger between 25 and 40 km. This indicates that the relative intensity of GWs over northwestern China and the Sea of Japan varies with height.

In summer (Figure 7b), the distribution of Ep at low latitudes is characterized by an upward–eastward column of large values from 20 to 40 km height, which extends nearly 4000 km eastward over this height range. Below 25 km, the column of large values appears in the area at 70–90°E, which corresponds to the GWs over the Indian peninsula. The column expands eastward with an increasing height reaching around 110°E above the height of 40 km and extending considerably farther vertically upward; this corresponds to the GWs over the Indo-China Peninsula. The zonal wind field distribution (dotted lines in Figure 7b) shows that the low-latitude stratosphere in summer is dominated by easterly winds, and in the easterly wind background field, the eastward-propagating GWs are significant, which is similar to the conclusion of Wang et al. [33] in a study of stratospheric GWs excited by Typhoon Likima. They found that during the upward propagation of GWs, the fluctuations propagating southward are filtered out, while the fluctuations propagating northward are retained owing to the presence of northerly winds in the background field.

3.2. The Generation and Propagation Mechanisms of Middle-Latitude GWs in Winter

Many studies have found that topography, strong convection, and the subtropical jet stream are all potential wave sources of stratospheric GWs [1,34]. In Section 3.1, areas with large Ep were found in northwestern China in winter, with a noteworthy vertical distribution: inclined from 30° to 40°N in the lower stratosphere below 25 km. To explore the formation mechanism of this phenomenon, we analyze the distribution of Ep at heights of 20 and 25 km (Figure 8). There are two significant centers of large Ep at these two heights. However, the latitudinal positions of the two high-value centers are different. At 20 km height (Figure 8a), one large value center is located above the Sichuan Basin in China near 30°N (referred to as box A), and the other is located near 40°N over the Sea of Japan (referred to as box B). The meridional position of the former center moves with increasing height. The large value center in box A moves northward to 40°N (Figure 8b), while the large-value center in box B moves a little. In the following, we mainly analyze the mechanism of GW generation in box A. The distribution of the wind field at 200 hPa (Figure 8a) shows an obvious subtropical jet stream at this altitude in winter. The center of the maximum value of Ep is located upstream of the jet stream center, which indicates that the stratospheric GWs in Box A may be related to the subtropical jet stream at 200 hPa. Therefore, the Box A region is selected to analyze the relationship between winter stratospheric GWs and the jet stream.

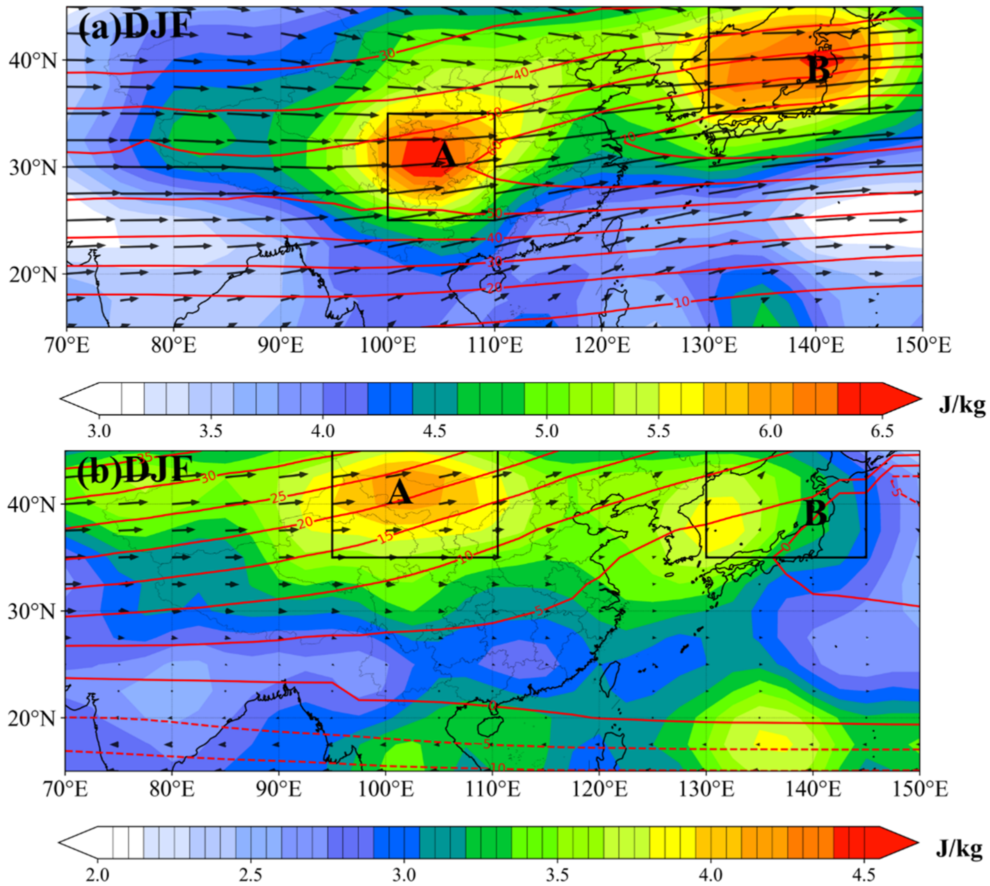

Figure 8. (**a**) Ep (shaded), wind speed (red contours, unit: m s^{-1}) and wind speed vectors (arrows) at 200 hPa. (**b**) All at 25 km.

Figure 9a shows the normalized time series of Ep at 20 km and the normalized time series of the 200 hPa wind speed in box A, which represents the intensity of GWs and the subtropical jet stream, respectively. Both are the 5-day averaged time series, and their correlation coefficient (the black and red solid line in Figure 9a) is 0.66. In order to eliminate the shorter time scale variation and to be able to clearly explain the relation of seasonal variation of Ep and the subtropical jet, we performed the Fourier transformation for the solid line in Figure 9a. The dashed line in Figure 9a represents the seasonal variation. The wind speed and Ep have similar characteristics of seasonal variation, both reaching maximum values in winter and minimum values in summer, and the correlation coefficient between the two dashed lines reaches 0.96. Figure 9b is the result of subtracting the dashed line from the solid line in Figure 9a, representing a shorter time scale variation without seasonal variation. The correlation coefficient between the two decreased to 0.22 but passed the 95% confidence test. From Figure 9b, the response of Ep to the wind field is better in winter and spring, and worse in autumn and summer, indicating that the subtropical jet stream in winter and spring has a greater impact on the stratospheric GWs than in summer and autumn. As the significant Ep in Box A has a good match with the center of the subtropical jet stream, Khan and Jin [35] pointed out that the jet stream is the main source of the stratosphere GW in winter. Chen et al. [24] also found that the correlation coefficient between subtropical jet stream and GWs intensity is lower in August and September. This area is located on the east side of the Tibetan Plateau. Zeng et al. [36] studied the orographic GWs activity over the Tibetan Plateau based on COSMIC data and found that the stratospheric GWs activity has a good correlation with elevation in the lower stratosphere. The region with high Ep values in winter and spring is located at 90–120°E (Figure 3 in Zeng et al. [36]), including the Box A region (Figure 9a). Therefore, the topography may be also the source of GWs in this area. The above analysis suggests that the lower stratosphere GWs appearing above the Sichuan Basin in winter is partially generated by the subtropical jet stream and topography, and more research about the wave sources is needed in the future.

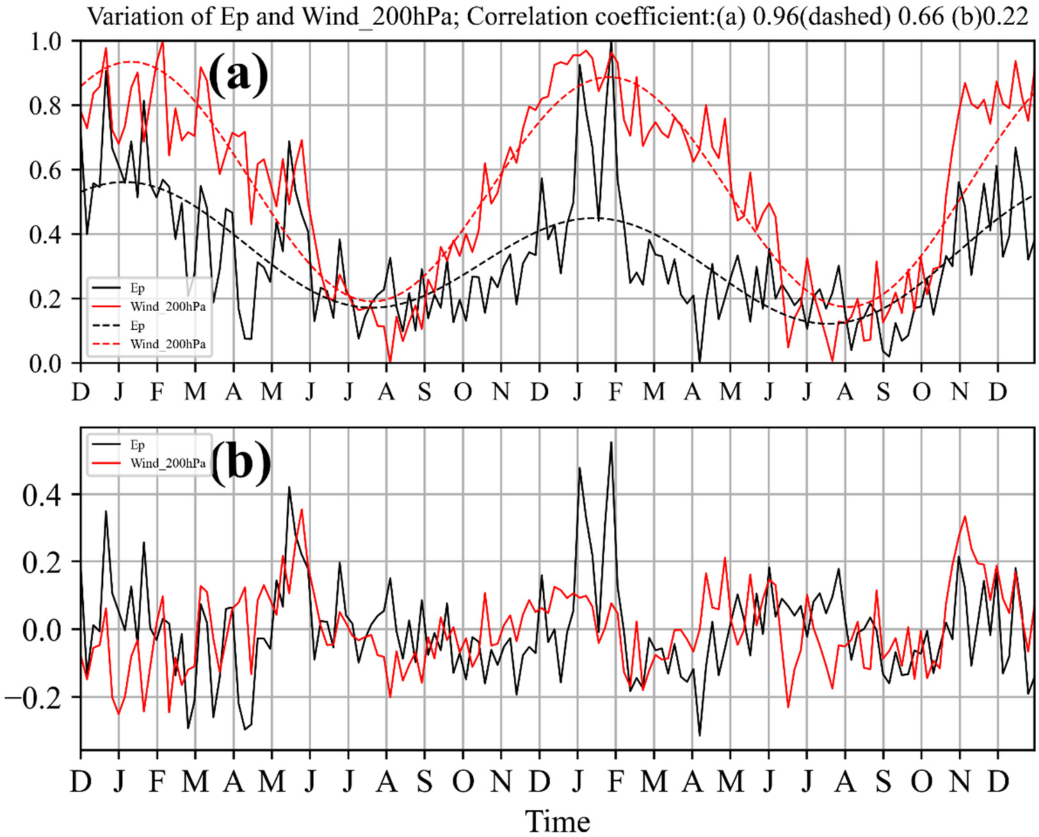

Figure 9. (**a**) Normalized time series of Ep at 20 km (black solid line), normalized time series of wind speed at 200 hPa (red solid line), the seasonal variations of Ep at 20 km (black dashed line) and wind speed at 200 hPa (red dashed line). (**b**) The shorter time scale variations of Ep (black line) and wind speed (red line) in box A.

Note that the center of the maximum Ep on the Sichuan Basin only appears below 22 km in the lower stratosphere. The position of significant Ep moves northward with height, and above 25 km, the center of the maximum value is stable around 40°N above 25 km (Figures 6a and 8). In order to explore the reasons for the northward shift of GWs, we analyze the distribution of the wind field in the stratosphere. The contour lines in Figure 6a represent the zonal winds. In the stratosphere above 20 km, the zonal wind at low latitudes (mid-latitudes) is easterly (westerly). In the 20–25 km height layer, the zonal westerly wind from 30° to 45°N gradually strengthens with latitude, and significant Ep propagates toward the large wind speed region, similar to that seen by Hindley et al. [17]. The zonal wind continues to increase in strength north of 45°N (not shown in the paper); however, the large values of Ep do not propagate farther northward, but instead propagate vertically at 40°N. This may be limited by COSMIC-2 data.

In previous studies, it was proposed that $\partial u/\partial y$ is the main reason for the northward propagation of GWs. Forbes et al. [37] studied the distribution of GWs in the tropical southern hemisphere and found that the GWs would move southward by 15° focusing toward the easterly jet core. They also found the $\partial u/\partial y$ plays a crucial role in the propagation of the GWs and explained the formation mechanism of this phenomenon using the theory of Dunkerton [38]. Dunkerton [38] gave the horizontal refraction as $dl/dt = -k\partial u/\partial y$ and when $dl/dt > 0$, GWs are refracted northward. Dunkerton's [38] view is that the stationary waves were rotated by the transverse horizontal shear and then propagated into the polar night jet. According to this method, we calculate the distribution of $\partial u/\partial y$ (Figure 10). It can be seen that $\partial u/\partial y$ from 30° to 42°N is significantly greater than the 0.9×10^{-5}/s, that is $\partial u/\partial y > 0$. $U \geq 0$ allows westward propagation of vertically propagating waves, indicating that $k \leq 0$. Thus, the horizontal refraction $dl/dt = -k\partial u/\partial y$ is greater than zero. This effect is to focus the GWs toward the north. During the upward propagation of the GWs excited by subtropical jet stream above the Sichuan Basin, they encounter a region of $\partial u/\partial y > 0$, and the column shifts to the north. Under this propagation mechanism, GWs should continue to move northward to the center of the jet stream. However, due to the limitations on the availability of the COSMIC-2 data, the propagation column north of 45°N cannot be seen. This shows that the activity of stratospheric GWs is not only related to the excitation source in the troposphere, but also to the background circulation in the stratosphere. GWs are sensitive to the stratosphere wind field, and the horizontal gradient value of the zonal wind can act as a refraction factor for stratospheric GWs.

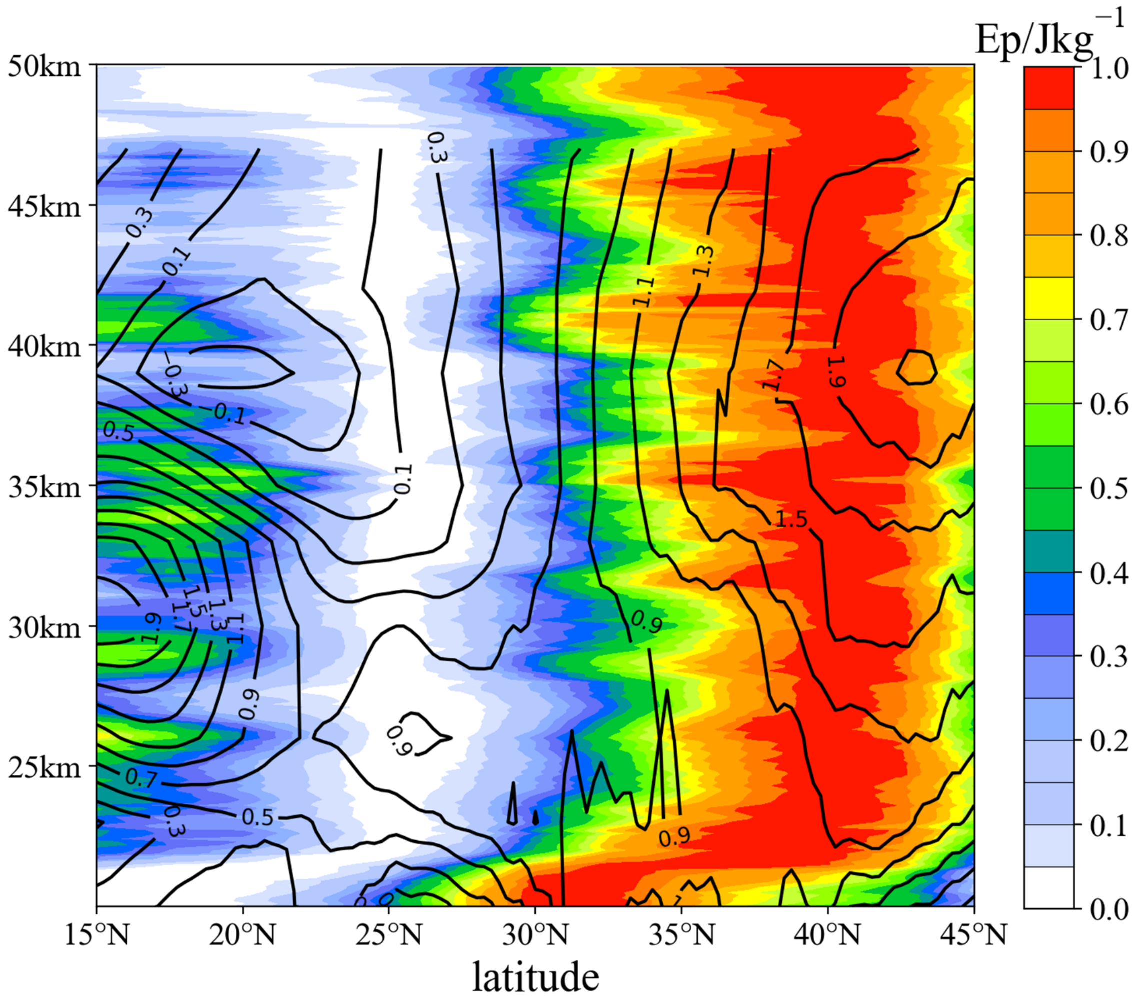

Figure 10. Seasonal mean $\partial u/\partial y$ (contours, units: 10^{-5}/s) and normalized Ep distribution along 105°E (±5°) (shaded, units: Jkg^{-1}).

4. Conclusions

COSMIC-2 dry temperature profile data for the past two years were used to study stratospheric GWs in the Asian monsoon region. The GW information was first extracted, and then, the Ep was calculated. The stratosphere at heights between 20 and 50 km was divided into the lower, middle, and high layers according to the vertical distribution of the area mean Ep. The horizontal distribution on these three layers, the vertical distribution, and its seasonal variation of Ep were analyzed. Then, the generation mechanism of mid-latitude GWs in winter was explored. The main conclusions are as follows:

The distribution of GW Ep in the stratosphere has obvious seasonal variation, which is more evident in the lower and middle layers than in the upper stratosphere. Significant Ep appears in the mid-latitude region around 40°N in winter, and the center of the maximum values lies over northwestern China and the Sea of Japan. In contrast, the most significant Ep appears in the tropical region south of 30°N in summer, and the large-value center of Ep is located over the Indian Peninsula. The Ep values in spring and autumn are smaller than those in winter and summer, and the distributions of Ep are similar in the lower stratosphere for these two seasons, with areas of large Ep in both middle and low latitudes. In addition to the areas with large Ep in the middle and low latitudes, there are also meridional belts of large Ep extending from south to north in the middle stratosphere in spring and summer. The area with large Ep in the upper layer is mainly in the middle latitudes, which indicates that the GWs in the tropics weaken rapidly during upward propagation, whereas the GWs in the middle latitudes tend to propagate into the upper layer.

The seasonal variation of GWs is accompanied by the evolution of the Asian monsoon. When the winter monsoon and the subtropical jet stream are at their strongest, the mid-latitude GWs are most significant. In summer, owing to the successive outbreaks of the East and South Asian monsoons, significant Ep first appears over the Indo-China Peninsula and the Indian Peninsula, and a belt of large Ep extends from the eastern mainland of China to the Korean Peninsula, which may be related to the northward movement of the rain belt in eastern China caused by the summer monsoon. In spring and autumn, when the winter monsoon and summer monsoon are in transition, the Ep values in the middle and low latitudes are weaker than those in summer and winter.

In winter, a GW column propagates northward and upward in the meridional range of the 100°E–110°E; thus, part of the wave source of GWs in the middle latitudes in winter can be traced back to the Sichuan Basin and even farther south. Our analysis finds that the GWs on the Sichuan Basin are the result of the subtropical jet stream and topography. After GWs enter the stratosphere, an area of positive $\partial u/\partial y$ appearing at 30–35°N in the lower layer of the stratosphere acts as a refraction factor that regulates the vertical propagation column of GWs. The GWs shift northward due to the refraction of $\partial u/\partial y$. However, due to the range limitation of COSMIC-2, it is not known whether the GW continues to move north. Therefore, it is necessary to combine other satellite data to study the propagation of GWs in future research.

Author Contributions: Conceptualization, T.Q. and L.Z.; methodology, T.Q. and L.Z.; software, T.Q.; validation, L.Z., T.Q., and Y.W.; formal analysis, T.Q. and L.Z.; investigation, T.Q.; resources, Y.W.; data curation, J.G.; writing—original draft preparation, T.Q.; writing—review and editing, L.Z., Y.W., and X.W.; visualization, T.Q.; supervision, L.Z.; project administration, L.Z.; funding acquisition, L.Z. and Y.W. All authors have read and agreed to the published version of the manuscript.

Funding: This research was funded by the National Natural Science Foundation of China grant 41975066, the National Natural Science Foundation for Young Scientists of China grant 42005053, the Science and Technology Innovation Program of Hunan Province grant 2021RC3072, and the Research Project of National University of Defense Technology grant ZK21-46.

Data Availability Statement: The COSMIC-2 level 2 dry temperature data are available at the COSMIC Data Analysis and Archive Center (https://cdaac-www.cosmic.ucar.edu/, accessed on 1 March 2022). The wind data are available at the European Centre for Medium-Range Weather Forecasts (https://cds.climate.copernicus.eu/, accessed on 1 March 2022).

Conflicts of Interest: The authors declare no conflict of interest. The funders had no role in the design of the study; in the collection, analyses, or interpretation of data; in the writing of the manuscript; or in the decision to publish the results.

References

1. Fritts, D.C.; Alexander, M.J. Gravity wave dynamics and effects in the middle atmosphere. *Rev. Geophys.* **2003**, *41*, 1003. [CrossRef]
2. Alexander, M.J.; Geller, M.; McLandress, C.; Polavarapu, S.; Preusse, P.; Sassi, F.; Sato, K.; Eckermann, S.; Ern, M.; Hertzog, A.; et al. Recent developments in gravity-wave effects in climate models and the global distribution of gravity-wave momentum flux from observations and models. *Q. J. R. Meteorol. Soc.* **2010**, *136*, 1103–1124. [CrossRef]
3. Zhang, S.D.; Yi, F.; Huang, C.M.; Zhou, Q.J. Latitudinal and seasonal variations of lower atmospheric inertial gravity wave energy revealed by US radiosonde data. *Ann. Geophys.* **2010**, *28*, 1065–1074. [CrossRef]
4. Wang, L.; Geller, M.J. Morphology of gravity-wave energy as observed from 4 years (1998–2001) of high vertical resolution U.S. radiosonde data. *J. Geophys. Res. Atmos.* **2003**, *108*, 4489. [CrossRef]
5. Tsuda, T.; Murayama, Y.; Yamamoto, M.; Kato, S.; Fukao, S. Seasonal variation of momentum flux in the mesosphere observed with the MU radar. *Geophys. Res. Lett.* **1990**, *17*, 725–728. [CrossRef]
6. Hertzog, A.; Boccara, G.; Vincent, R.A.; Vial, F.; Cocquerez, P. Estimation of Gravity Wave Momentum Flux and Phase Speeds from Quasi-Lagrangian Stratospheric Balloon Flights. Part II: Results from the Vorcore Campaign in Antarctica. *J. Atmos. Sci.* **2008**, *65*, 3056–3070. [CrossRef]
7. Hertzog, A.; Alexander, J.M.; Plougonven, R. On the intermittency of gravity wave momentum flux in the stratosphere (Article). *J. Atmos. Sci.* **2012**, *69*, 3433–3448. [CrossRef]
8. Eckermann, S.D.; Hirota, I.; Hocking, W.K. Gravity wave and equatorial wave morphology of the stratosphere derived from long-term rocket soundings. *Q. J. R. Meteorol. Soc.* **1995**, *121*, 149–186. [CrossRef]
9. Anthes, R.A.; Ector, D.; Hunt, D.C.; Kuo, Y.H.; Rocken, C.; Schreiner, W.S.; Sokolovskiy, S.V.; Syndergaard, S.; Wee, T.K.; Zeng, Z.J. The COSMIC/FORMOSAT-3 Mission: Early Results. *Bull. Am. Meteorol. Soc.* **2008**, *89*, 313–333. [CrossRef]
10. Ware, R.; Rocken, C.; Solheim, F.; Exner, M.; Schreiner, W.; Anthes, R.; Feng, D.; Herman, B.; Gorbunov, M.; Sokolovskiy, S.J. GPS Sounding of the Atmosphere from Low Earth Orbit: Preliminary Results. *Bull. Am. Meteorol. Soc.* **1996**, *77*, 19–40. [CrossRef]
11. Ratnam, V.M.; Tetzlaff, G.; Jacobi, C. Global and Seasonal Variations of Stratospheric Gravity Wave Activity Deduced from the CHAMP/GPS Satellite. *J. Atmos. Sci.* **2004**, *61*, 1610–1620. [CrossRef]
12. Alexander, S.P.; Tsuda, T.; Kawatani, Y.; Takahashi, M. Global distribution of atmospheric waves in the equatorial upper troposphere and lower stratosphere: COSMIC observations of wave mean flow interactions. *J. Geophys. Res.* **2008**, *113*, D24115. [CrossRef]
13. Tsuda, T.; Nishida, M.; Rocken, C.; Ware, R.H. A global morphology of gravity wave activity in the stratosphere revealed by the GPS occultation data (GPS/MET). *J. Geophys. Res.* **2000**, *105*, 7257–7273. [CrossRef]
14. Xu, X.H.; Yu, D.C.; Luo, J. The Spatial and Temporal Variability of Global Stratospheric Gravity Waves and Their Activity during Sudden Stratospheric Warming Revealed by COSMIC Measurements. *Adv. Atmos. Sci.* **2018**, *35*, 1533–1546. [CrossRef]
15. Wang, L.; Alexander, M.J. Global estimates of gravity wave parameters from GPS radio occultation temperature data. *J. Geophys. Res. Atmos.* **2010**, *115*. [CrossRef]
16. Faber, A.; Llamedo, P.; Schmidt, T.; Torre, A.D.; Wickert, J. On the determination of gravity wave momentum flux from GPS radio occultation data. *Atmos. Meas. Tech.* **2013**, *11*, 3169–3180. [CrossRef]
17. Hindley, N.P.; Wright, C.J.; Smith, N.D.; Mitchell, N.J. The southern stratospheric gravity-wave hot spot: Individual waves and their momentum fluxes measured by COSMIC GPS-RO. *Atmos. Chem. Phys. Discuss.* **2015**, *15*, 3173–3217. [CrossRef]
18. Šacha, P.; Kuchař, A.; Jacobi, C.; Pišoft, P. Enhanced internal gravity wave activity and breaking over the northeastern Pacific-eastern Asian region. *Atmos. Chem. Phys.* **2015**, *15*, 13097–13112. [CrossRef]
19. Fjeldbo, G.; Kliore, A.J.; Eshleman, V.R. The Neutral Atmosphere of Venus as Studied with the Mariner V Radio Occultation Experiments. *Atmos. J.* **1971**, *76*, 123. [CrossRef]
20. Ho, S.P.; Zhou, X.; Shao, X.; Zhang, B.; Adhikari, L.; Kireev, S.; He, Y.; Yoe, J.G.; Xia-Serafino, W.; Lynch, E. Initial Assessment of the COSMIC-2/FORMOSAT-7 Neutral Atmosphere Data Quality in NESDIS/STAR Using in Situ and Satellite Data. *Remote Sens.* **2020**, *12*, 4099. [CrossRef]
21. Schreiner, W.S.; Weiss, J.P.; Anthes, R.A.; Braun, J.; Chu, V.; Fong, J.; Hunt, D.; Kuo, Y.H.; Meehan, T.; Serafino, W.; et al. COSMIC-2 Radio Occultation Constellation: First Results. *Geophys. Res. Lett.* **2020**, *47*, e2019GL086841. [CrossRef]
22. Zhang, S.D.; Yi, F. Latitudinal and seasonal variations of inertial gravity wave activity in the lower atmosphere over central China. *J. Geophys. Res. Atmos.* **2007**, *112*. [CrossRef]
23. Bai, Z.X.; Bian, J.C.; Chen, H.B.; Chen, L. Inertial gravity wave parameters for the lower stratosphere from radiosonde data over China. *Sci. China* **2017**, *60*, 328–340. [CrossRef]
24. Chen, L.; Bian, J.; Liu, Y.; Bai, Z.; Qiao, S. Statistical analysis of inertial gravity wave parameters in the lower stratosphere over Northern China. *Clim. Dyn.* **2019**, *52*, 563–575. [CrossRef]
25. Wang, Y.; Zhang, L.; Zhang, Y.; Guan, J. Effects of Tropospheric Vertical Wind Shear on Gravity Waves Generated by Tropical Cyclones. *Geophys. Res. Lett.* **2019**, *46*, 4523–4530. [CrossRef]
26. Wang, X.; Zhang, L.; Wang, Y.; Zhang, Y. The Influencing Mechanism of a Mid-Latitude Westerly Trough on Stratospheric Gravity Waves Generated by Typhoon Lekima (2019). *Geophys. Res. Lett.* **2022**, *49*, e2021GL097544. [CrossRef]
27. Randel, W.J.; Wu, F.; Podglajen, A. Equatorial Waves, Diurnal Tides and Small-Scale Thermal Variability in the Tropical Lower Stratosphere From COSMIC-2 Radio Occultation. *J. Geophys. Res.* **2021**, *126*, e2020JD033969. [CrossRef]

28. Hersbach, H.; Bell, B.; Berrisford, P.; Hirahara, S.; Horányi, A.; Muñoz-Sabater, J.; Nicolas, J.; Peubey, C.; Radu, R.; Schepers, D.; et al. The ERA5 global reanalysis. *Q. J. R. Meteorol. Soc.* **2020**, *146*, 1999–2049. [CrossRef]
29. Strelnikova, I.; Almowafy, M.; Baumgarten, G.; Baumgarten, K.; Ern, M.; Gerding, M.; Lubken, F.J. Seasonal Cycle of Gravity Wave Potential Energy Densities from Lidar and Satellite Observations at 54° and 69°N. *J. Atmos. Sci.* **2021**, *78*, 1359–1386. [CrossRef]
30. Wang, L.; Alexander, M.J. Gravity wave activity during stratospheric sudden warmings in the 2007-2008 Northern Hemisphere winter(Article). *J. Geophys. Res. Atmos.* **2009**, *114*. [CrossRef]
31. John, S.R.; Kumar, K.K. A discussion on the methods of extracting gravity wave perturbations from space-based measurements. *Geophys. Res. Lett.* **2013**, *40*, 2406–2410. [CrossRef]
32. Chen, C.; Zhao, N.; Yue, T.; Guo, J. A generalization of inverse distance weighting method via kernel regression and its application to surface modeling. *Arab. J. Geosci.* **2015**, *8*, 6623–6633. [CrossRef]
33. Wang, X.; Zhang, L.; Wang, Y.; Zhang, Y. Influences of the Mid-Latitude Westerly Trough on Stratospheric Gravity Waves Generated by Typhoon Lekima (2019). *J. Geophys. Res. Atmos.* **2021**, *126*, e2021JD035399. [CrossRef]
34. Zhang, S.; Yi, F.; Huang, C.; Huang, K.; Gan, Q.; Zhang, Y.; Gong, Y. Latitudinal and altitudinal variability of lower atmospheric inertial gravity waves revealed by U.S. radiosonde data(Article). *J. Geophys. Res. Atmos.* **2013**, *118*, 7750–7764. [CrossRef]
35. Khan, A.; Jin, S. Gravity wave activities in Tibet observed by COSMIC GPS radio occultation(Article). *Geod. Geodyn.* **2018**, *9*, 504–511. [CrossRef]
36. Zeng, X.; Xue, X.; Dou, X.; Liang, C.; Jia, M. COSMIC GPS observations of topographic gravity waves in the stratosphere around the Tibetan Plateau. *Sci. China-Earth Sci.* **2017**, *60*, 188–197. [CrossRef]
37. Forbes, J.M.; Zhang, X.; Randall, C.E.; France, J.; Harvey, V.L.; Carstens, J.; Bailey, S.M. Troposphere-Mesosphere Coupling by Convectively Forced Gravity Waves During Southern Hemisphere Monsoon Season as Viewed by AIM/CIPS. *J. Geophys. Res. Space Phys.* **2021**, *126*, e2021JA029734. [CrossRef]
38. Dunkerton, T.J. Inertia–Gravity Waves in the Stratosphere. *J. Atmos. Sci.* **1984**, *41*, 3396–3404. [CrossRef]